minerals

MDPI

Article

Calcium Carbonate Precipitation Behavior in the System Ca-Me^{2+}-CO_3-H_2O (Me^{2+} = Co, Ni, Cu, Fe): Ion Incorporation, Effect of Temperature and Aging

Oleg S. Vereshchagin *, Irina A. Chernyshova, Maria A. Kuz'mina and Olga V. Frank-Kamenetskaya

Institute of Earth Sciences, Saint Petersburg State University, Universitetskaya Emb. 7/9, 199034 St. Petersburg, Russia; i.a.chernyshova@yandex.ru (I.A.C.); ofrank-kam@mail.ru (O.V.F.-K.)
* Correspondence: o.vereshchagin@spbu.ru

Abstract: Crystalline calcium carbonates (CCCs) are among the most widespread minerals on the Earth's surface and play a crucial role in the global carbon cycle, heavy metal sorption and incorporation. Among the numerous factors that influence the precipitation of CCCs from solution, the most determinant are the presence of additives in the mineral-forming medium, temperature, and crystallization time (aging time). The current work fills the gaps in the study of calcium carbonate crystallization from heavy metal (Me^{2+} = Co, Ni, Cu Fe)-containing solutions (Me^{2+}/Ca 0.005–1.600) at different temperatures (3 and 23 °C) and aging times (21–158 days). The resulting precipitates were studied using optical and scanning electron microscopy, powder X-ray diffraction and energy-dispersive X-ray spectroscopy. Three crystalline calcium carbonates (synthetic analogues of calcite, aragonite and monohydrocalcite), as well as amorphous carbonate (AC), were found in the resulting precipitates. Temperature and aging time have a considerable effect on the phase composition, morphology and heavy metal content in CCCs. Low temperature (3 °C) and short aging times are generally favorable for the formation of monohydrocalcite and amorphous carbonate, while calcite tends to form at a higher temperature (23 °C) and in long-term experiments. Heavy metals can be incorporated into the calcite/monohydrocalcite crystal lattice in sufficient amounts, while aragonite can host a very small amount of Me^{2+} (or none). Calcite can concentrate Co (up to ~0.25 atoms per formula unit (apfu)) and Ni/Cu (up to ~0.05 apfu), while its Fe content is very close to the detection limits. Calcite precipitated at a higher Me^{2+}/Ca ratio and temperature (23 °C) contains less Me^{2+} compared to calcite precipitated at a lower Me^{2+}/Ca ratio and temperature (3 °C). Monohydrocalcite can host up to ~0.1 apfu of Co/Ni/Cu with no detectable preference for Me^{2+}. The amount of Me^{2+} in monohydrocalcite decreases as aging time or temperature increases. It is worth noting that AC is the main carrier of heavy metals in the system being investigated and it should be considered the main host phase in heavy metal adsorption from aqueous solutions. The results obtained can be used to solve environmental issues and in mineral resource management.

Keywords: monohydrocalcite; aragonite; calcite; malachite; synthesis; Cu; Ni; Co; Fe

Citation: Vereshchagin, O.S.; Chernyshova, I.A.; Kuz'mina, M.A.; Frank-Kamenetskaya, O.V. Calcium Carbonate Precipitation Behavior in the System Ca-Me^{2+}-CO_3-H_2O (Me^{2+} = Co, Ni, Cu, Fe): Ion Incorporation, Effect of Temperature and Aging. *Minerals* **2023**, *13*, 1497. https://doi.org/10.3390/min13121497

Academic Editors: Mariella Rivas and Dayana Arias

Received: 17 October 2023
Revised: 17 November 2023
Accepted: 27 November 2023
Published: 29 November 2023

1. Introduction

Crystalline calcium carbonates (CCCs) are among the most widespread minerals on the Earth's surface (e.g., [1]), in particular, in oceans (e.g., [2]). They are the most commonly encountered biominerals (e.g., [3]) and play a crucial role in the global carbon cycle (e.g., [4]). A substantial part of the anthropogenic CO_2 has been absorbed by the oceans, which has changed carbonate ion availability and led to ocean acidification. Acidification affects the biogeochemical cycles of elements [5], including those of minor elements (e.g., [6]). These cycles are known to be CCC-type dependent, as different CCCs have different capacities to host these elements.

Five CCC minerals are known: three anhydrous polymorphs of $CaCO_3$ (calcite, aragonite and vaterite) and two hydrated phases—$CaCO_3 \cdot H_2O$ (monohydrocalcite) and

$CaCO_3 \cdot 6H_2O$ (ikaite). Calcium is six-coordinated in the calcite crystal structure (e.g., [7]), eight-coordinated in ikaite, monohydrocalcite and nine-coordinated in aragonite crystal structures (e.g., [8,9]). This indicates the different ability of these minerals to capture "foreign" cations.

Calcite should be the only stable phase under the Earth's surface conditions (e.g., [10–12]), but aragonite, vaterite, monohydrocalcite and ikaite are also present both as abiogenic phases and biominerals (e.g., [11]).

Both biogenic and abiogenic CCCs could also serve as a chemical archive of the conditions in which they were formed (e.g., [13,14]) and provide one of the most comprehensive geochemical records of the environmental and climatic conditions occurring at the time of mineral formation (e.g., [15,16]). However, most studies are focused on calcite (e.g., [17]), there is limited information available on the mechanisms of trace element incorporation into aragonite (e.g., [18–20]), and there are almost no data concerning hydrated calcium carbonates (monohydrocalcite and ikaite). Among the numerous factors influencing CCC precipitation, the most determinant are probably the presence of (cation) additives in the mineral-forming medium, temperature and crystallization time (aging time) (e.g., [21,22]).

Heavy metal content in rivers and lakes all over the world has dramatically increased over the past 50 years [23], making heavy metal pollution of surface water a global environmental problem (e.g., [24]). Heavy metals generally include metals with relatively high densities, which is the case with the first-row transition metals. It is important to note that most of the first-row transition metals are toxic for a number of living organisms (e.g., [25–27]). Cation additives have a considerable effect on CCC growth and have attracted the attention of researchers for decades (e.g., [12,21,28]). CCC crystallization in Co- (e.g., [29,30]), Ni- (e.g., [20,31]), Cu- (e.g., [21,32,33]) and Fe-rich (e.g., [34–36]) systems was studied previously. It was shown that the presence of some heavy metals (e.g., Co, Fe) violates the normal sequence of calcium carbonate crystallization (e.g., [20,30,37,38]). However, it was found that the effect of cations is very different due to the possibility of their incorporation into the structure of CCCs/the sorption on CCC surface, as well as different behavior in aqueous solutions (e.g., [20,21,29]). In addition, CCCs typically form small crystals (<5 μm) and have complex intergrowths (e.g., spheres) in heavy metal-rich systems, making it impossible to obtain direct data on their chemical composition using X-ray spectroscopy (EDX/WDX; typical spot size ~3 μm) or inductively coupled plasma mass spectrometry (LA-ICP MS; typical spot size ~50–70 μm). The main method that could reveal the occurrence of impurities in CCCs is the measurement of the unit cell parameters of the phases under consideration, but neither the Inorganic Crystal Structure Database (ICSD) nor the Powder X-ray Diffraction Database contains information on the unit cell parameters of CCCs enriched with heavy metals.

Temperature-dependent studies are especially important when biomineral formation and surface processes are modeled. The precipitation of hydrated CCCs (monohydrocalcite and ikaite) tends to be favored by low (<7 °C) temperatures (e.g., [11]), but anhydrous CCCs (e.g., aragonite) could also form instead of calcite under such conditions (e.g., [39]). However, the influence of low temperatures (<25 °C) has received little attention so far since the study of such systems requires a long crystallization time (e.g., [22]).

Aging time is crucial for CCC formation (e.g., [22,40]) and their chemical composition (e.g., [22,30,40]). It has been found that metastable CCC (e.g., vaterite/aragonite/monohydrocalcite) formation is favored by short aging time (<1 day, e.g., [30,40]), while long crystallization time can lead to the formation of both stable (calcite) and metastable (monohydrocalcite) CCCs (e.g., [22,30,40]). Thus, additional experiments are needed to establish the effect of crystallization time on the phase composition of sediments and the chemical composition of CCCs.

The current work fills the gaps in the study of calcium carbonate crystallization from heavy metal (Me^{2+} = Co, Ni, Cu, Fe)-containing solutions at different temperatures and aging times. Practically, the issues of incorporation of Me^{2+} into the CCC crystal lattice, temperature effect, and aging time effect were considered.

2. Materials and Methods

2.1. Synthesis

Syntheses were carried out by a precipitation method from aqueous solutions at different temperatures, Me^{2+}/Ca ratios and aging times. Changes in the unit cell parameters and unit cell volume of the CCCs were used to identify the incorporation of heavy metals in the CCCs [22].

Synthesis was conducted in a closed volume of an aqueous solution by the rapid addition (under constant and vigorous stirring) of $CaCl_2$ (99%, Vekton (Saint-Petersburg, Russia)) + $CoCl_2 \cdot 6H_2O$ (99%, Vekton)/$NiCl_2 \cdot 6H_2O$ (99%, Vekton)/$CuCl_2 \cdot 2H_2O$ (99%, Vekton)/$FeSO_4 \cdot 7H_2O$ (99%, Vekton) solution to a 20 mM Na_2CO_3 (99%, Vekton)/$NaHCO_3$ (99%, Vekton)/NaOH (99%, Vekton) solution. The Na_2CO_3/$NaHCO_3$/NaOH ratio was used to change the pH of the solution. The Ca/CO_3 ratio was set as 0.5 (Tables 1 and 2). Two series of syntheses were performed at different temperatures and Me^{2+}/Ca ratios (Me^{2+} = Co, Ni, Cu, Fe): 55 syntheses at a temperature of 3 °C (Me^{2+}/Ca 0.005–1.600, Table 1) and 26 syntheses at a temperature of 23 °C (Me^{2+}/Ca 0.005–1.300, Table 2). Syntheses were conducted for 21–158 days (Tables 1 and 2) and were stopped as the mother solution became clear and a layer on the bottom of the beaker was formed. The resulting precipitates were filtered, washed with deionized water several times and dried at room temperature in the air for 24 h.

Table 1. Experimental conditions for the carbonate syntheses carried out at 3 °C.

No.	Sample Name (CAV)	Exposure Time, Day	Me^{2+}, mmol/L	Ca, mmol/L	CO_3, mmol/L	Me^{2+}/Ca, Solution	pH Initial	pH Final
				Me^{2+} = Co				
1	43	21	10.000	10.000	20.000	1.000	7.50	7.95
2	42	21	5.000	10.000	20.000	0.500	8.55	8.68
3	49	158	3.320	10.000	20.000	0.300	8.75	8.73
4	52	158	4.640	14.000	28.000	0.300	10.05	9.90
5	46	57	2.000	10.000	20.000	0.200	8.60	8.20
6	54	31	2.800	14.000	28.000	0.200	9.44	9.33
7	55	31	2.100	14.000	28.000	0.150	9.54	8.80
8	41A	34	2.800	14.000	28.000	0.120	8.50	8.32
9	97	103	1.612	14.000	28.000	0.115	9.38	9.65
10	71	57	1.540	14.000	28.000	0.110	9.80	9.73
11	96	103	1.472	14.000	28.000	0.105	10.03	9.75
12	69	37	1.400	14.000	28.000	0.100	9.23	8.41
13	70	37	1.400	14.000	28.000	0.100	8.77	8.54
14	72	57	1.400	14.000	28.000	0.100	9.73	9.53
15	56	31	1.400	14.000	28.000	0.100	9.61	9.58
16	95	103	1.332	14.000	28.000	0.095	9.96	9.84
17	73	57	1.260	14.000	28.000	0.090	9.50	9.53
18	40A	34	1.200	14.000	28.000	0.080	9.15	8.93
19	68	37	0.700	14.000	28.000	0.050	8.98	8.52
20	67	37	0.700	14.000	28.000	0.050	9.37	8.62
21	53	31	0.700	14.000	28.000	0.050	9.63	9.76
				Me^{2+} = Ni				
22	57	31	16.000	10.000	20.000	1.600	7.55	7.82
23	58	31	14.000	14.000	28.000	1.400	7.83	7.75
24	59	31	12.000	10.000	20.000	1.200	7.94	8.06
25	66	37	11.000	10.000	20.000	1.100	8.08	8.20
26	74	57	10.500	10.000	20.000	1.050	8.90	9.33
27	45	57	10.000	10.000	20.000	1.000	8.75	9.10
28	98	114	12.000	12.000	24.000	1.000	8.85	9.31
29	75	57	10.000	10.000	20.000	1.000	8.45	9.02
30	76	57	9.500	10.000	20.000	0.950	8.50	9.09

Table 1. *Cont.*

No.	Sample Name (CAV)	Exposure Time, Day	Me^{2+}, mmol/L	Ca, mmol/L	CO_3, mmol/L	Me^{2+}/Ca, Solution	pH Initial	pH Final
31	65	37	9.000	10.000	20.000	0.900	8.41	7.75
32	60	31	8.000	10.000	20.000	0.800	8.63	8.33
33	51	158	7.000	14.000	28.000	0.500	8.80	8.46
				Me^{2+} = Cu				
34	62	31	15.000	10.000	20.000	1.500	5.44	7.49
35	64	37	11.000	10.000	20.000	1.100	6.35	7.87
36	61	31	10.000	10.000	20.000	1.000	6.56	8.10
37	77	57	9.500	10.000	20.000	0.950	6.60	9.06
38	63	37	9.000	10.000	20.000	0.900	6.93	7.74
39	99	114	10.800	12.000	24.000	0.900	7.50	9.34
40	78	57	9.000	10.000	20.000	0.900	6.75	9.25
41	79	57	8.500	10.000	20.000	0.850	6.80	9.26
42	44	57	5.000	10.000	20.000	0.500	6.95	8.50
43	47	158	3.000	10.000	20.000	0.300	7.48	8.87
44	50	158	2.800	14.000	28.000	0.200	7.55	9.03
				Me^{2+} = Fe				
45	154	44	5.000	10.000	20.000	0.500	9.30	10.49
46	153	44	4.000	10.000	20.000	0.400	9.50	10.40
47	152	44	3.000	10.000	20.000	0.300	10.15	9.84
48	151	44	2.000	10.000	20.000	0.200	10.35	10.81
49	150	44	1.000	10.000	20.000	0.100	10.50	10.69
50	124	66	0.500	10.000	20.000	0.050	11.15	10.40
51	123	66	0.300	10.000	20.000	0.030	11.40	11.02
52	138	90	0.252	10.000	20.000	0.025	11.05	9.70
53	137	90	0.152	10.000	20.000	0.015	11.11	9.99
54	122	66	0.100	10.000	20.000	0.010	11.20	10.09
55	136	90	0.052	10.000	20.000	0.005	11.05	9.78

Table 2. Experimental conditions for the carbonate syntheses carried out at 23 °C.

No.	Sample Name (CME)	Exposure Time, Day	Me^{2+}, mmol/L	Ca, mmol/L	CO_3, mmol/L	Me^{2+}/Ca, Solution	pH Initial	pH Final
				Me^{2+} = Co				
1	20	42	5.000	10.000	20.000	0.500	9.74	8.21
2	21	42	4.000	10.000	20.000	0.400	9.92	9.53
3	1	30	5.000	15.000	30.000	0.300	9.50	8.40
4	25	44	2.000	10.000	20.000	0.200	10.36	9.74
5	26	44	1.000	10.000	20.000	0.100	10.45	8.98
				Me^{2+} = Ni				
6	22	42	13.000	10.000	20.000	1.300	7.93	7.82
7	27	44	11.000	10.000	20.000	1.100	8.18	8.24
8	2	30	15.000	15.000	30.000	1.000	8.20	8.00
9	28	44	9.000	10.000	20.000	0.900	8.40	7.95
10	23	42	8.000	10.000	20.000	0.800	8.31	7.89
11	29	44	6.000	10.000	20.000	0.600	9.34	8.52
				Me^{2+} = Cu				
12	30	44	12.000	10.000	20.000	1.200	6.27	8.13
13	31	44	9.000	10.000	20.000	0.900	6.91	8.06
14	32	44	5.400	10.000	20.000	0.700	8.80	7.99
15	24	42	6.000	10.000	20.000	0.600	8.72	7.74

Table 2. *Cont.*

No.	Sample Name (CME)	Exposure Time, Day	Me^{2+}, mmol/L	Ca, mmol/L	CO_3, mmol/L	Me^{2+}/Ca, Solution	pH Initial	pH Final
				Me^{2+} = Fe				
16	111	41	5.000	10.000	20.000	0.500	9.20	9.66
17	110	40	4.000	10.000	20.000	0.400	9.50	10.00
18	109	40	3.000	10.000	20.000	0.300	10.20	10.37
19	108	40	2.000	10.000	20.000	0.200	10.40	10.60
20	107	40	1.000	10.000	20.000	0.100	10.60	10.99
21	81	64	0.500	10.000	20.000	0.050	10.75	11.15
22	80	64	0.300	10.000	20.000	0.030	10.50	11.07
23	95	94	0.252	10.000	20.000	0.025	11.20	11.14
24	94	94	0.152	10.000	20.000	0.015	11.03	10.77
25	79	64	0.100	10.000	20.000	0.010	10.95	11.36
26	93	94	0.052	10.000	20.000	0.005	11.15	11.39

2.2. Characterization Methods

The resulting precipitates (after washing and drying) were studied by optical microscopy, followed by powder X-ray diffraction (PXRD). After that, precipitates were studied by scanning electron microscopy (SEM) and energy-dispersive X-ray spectroscopy (EDX).

The main method that can reveal the occurrence of impurities in CCCs is the measurement of the unit cell parameters of the phases under consideration.

Optical microscopy. The morphology and optical properties (e.g., color, luster) of the synthesized products were studied using a DM 2500P (Leica, Germany) polarizing light microscope.

Powder X-ray diffraction. PXRD was used to identify the phase composition of the precipitation and determine unit cell parameters (UCPs) of newly formed phases. The regularities of change in UCPs were used in the study of the possibility of heavy metal incorporation into CCCs. PXRD patterns of samples were recorded on a Miniflex II diffractometer (Rigaku, Japan) with CoKα/CuKα radiation (2-theta range 5–110°, velocity 2°/min, step size 0.02°, Bragg-Brentano geometry). Phase identification was carried out using the PDF-2 Database. Subsequent quantitative phase content analyses of precipitates were carried out using the full-profile method using Bruker TOPAS v. 5.0 software. Unit cell parameters (for samples with a single-phase content >90%) were determined using an Ultima IV high-resolution diffractometer (Rigaku, Japan) with CuKα radiation (2-theta range 5–120°, velocity 1°/min, step size 0.02°, Bragg-Brentano geometry; PSD D-Tex Ultra detector) with internal standard (Ge).

Scanning electron microscopy and energy-dispersive X-ray spectroscopy. SEM, together with EDX spectroscopy, was used to study the morphology and chemical composition of newly formed phases by means of an S-3400N (Hitachi, Japan) SEM equipped with an AzTec Energy X-Max 20 EDX spectrometer (Oxford Instruments, UK) with the following parameters: 20 kV accelerating voltage, 1 nA beam current and 30 s data collection time (excluding dead time).

3. Results

3.1. Resulting Phase Composition and Crystal (Micro) Morphology

PXRD revealed four crystalline carbonates (synthetic analogues of calcite (space group (SpGr) *R*-3*c*, ideally $CaCO_3$), aragonite (SpGr *Pmcn*, ideally $CaCO_3$), monohydrocalcite (SpGr $P3_1$, ideally $CaCO_3 \cdot H_2O$), malachite (SpGr $P2_1/b$, ideally $Cu_2(CO_3)(OH)_2$)) and two oxides (synthetic analogues of goethite (SpGr *Pbnm*, ideally FeO(OH)) and magnetite (SpGr *Fd*3*m*, ideally $FeFe_2O_4$)) in resulting precipitates (Tables 3 and 4). Despite the long crystallization time, an amorphous carbonate (AC) was typically present (Tables 3 and 4).

Table 3. Phase composition (PXRD data) of precipitates synthesized at 3 °C and UCPs of the main CCCs.

No. *	Sample Name (CAV)	Me^{2+}/Ca, Solution	Crystalline Phase Composition, %	Amorphous Phase	Unit Cell Parameters, Å		
					a	*b*	*c*
			Me^{2+} = Co				
1	43	1.000	Arg 91 Cal 9	□	4.959(2)	7.964(3)	5.743(2)
2	42	0.500	Cal 81 Arg 19	+			
3	49	0.300	Cal 90 Arg 10	-	4.970(3)	=*a*	16.930(2)
4	52	0.300	Cal 97 Arg 3	-	4.960(3)	=*a*	16.876(2)
5	46	0.200	Cal 100	-	4.979(3)	=*a*	16.981(2)
6	54	0.200	Cal 78 Arg 22	+			
7	55	0.150	Cal 63 Arg 37	+			
8	41A	0.120	Mhcal 86 Arg 14	+			
9	97	0.115	Cal 72 Arg 28	±			
10	71	0.110	Mhcal 100	-	10.553(3)	=*a*	7.542(2)
11	96	0.105	Mhcal 70 Cal 27 Arg 3	±			
12	69	0.100	Arg 65 Mhcal 23 Cal 12	+			
13	70	0.100	Mhcal 98 Arg 2	±	10.536(4)	=*a*	7.534(2)
14	72	0.100	Mhcal 100	±	10.545(3)	=*a*	7.539(2)
15	56	0.100	Cal 66 Arg 34	+			
16	95	0.095	Cal 77 Arg 23	-			
17	73	0.090	Mhcal 52 Cal 28 Arg 20	□			
18	40A	0.080	Cal 60 Arg 35 Mhcal 5	+			
19	68	0.050	Cal 81 Arg 19	-			
20	67	0.050	Cal 95 Arg 5	-	4.966(2)	=*a*	16.911(3)
21	53	0.050	Cal 94 Arg 6	-	4.969(2)	=*a*	16.926(3)
			Me^{2+} = Ni				
22	57	1.600	-	■			
23	58	1.400	-	■			
24	59	1.200	Arg 10 Cal 90	■			
25	66	1.100	Arg 66 Cal 34	■			
26	74	1.050	Cal 90 Arg 10	+	4.989(3)	=*a*	17.054(4)
27	45	1.000	Mhcal 64 Cal36	■			
28	98	1.000	Cal 85 Mhcal 15	±			
29	75	1.000	Cal 100	■			
30	76	0.950	Cal 99 Arg 1	±	4.987(3)	=*a*	17.040(4)
31	65	0.900	Cal 84 Arg 16	+			
32	60	0.800	Cal 69 Arg 31	±			
33	51	0.500	Cal 96 Mhcal 4	±	4.985(3)	=*a*	17.020(3)
			Me^{2+} = Cu				
34	62	1.500	Mlc 100	±	9.536(2)	11.870(4)	3.270(1)
35	64	1.100	Mlc 78 Arg 22	+			
36	61	1.000	Amorphous/Mhcal	■			
37	77	0.950	Cal 87 Mhcal 7 Arg 6	+			
38	63	0.900	Mhcal 100	□	10.547(4)	=*a*	7.549(2)
39	99	0.900	Cal 54 Mhcal 46	□			
40	78	0.900	Cal 96 Arg 4	-	4.971(3)	=*a*	16.991(3)
41	79	0.850	Cal 86 Arg 14	-	4.979(3)	=*a*	17.022(4)
42	44	0.500	Cal 100	-	4.976(2)	=*a*	17.012(3)
43	47	0.300	Cal 100	-	4.977(2)	=*a*	17.004(3)
44	50	0.200	Cal 100	-	4.976(2)	=*a*	16.989(3)
			Me^{2+} = Fe				
45	154	0.500	Cal 72 Gth 28	±			
46	153	0.400	Cal 78 Gth 22	±			
47	152	0.300	Cal 82 Mgt 18	±			
48	151	0.200	Cal 84 Mgt 16	-			

Table 3. *Cont.*

No. *	Sample Name (CAV)	Me^{2+}/Ca, Solution	Crystalline Phase Composition, %	Amorphous Phase	Unit Cell Parameters, Å		
					a	*b*	*c*
49	150	0.100	Cal 100	-	4.993(2)	=*a*	17.051(3)
50	124	0.050	Cal 100	-	4.992(2)	=*a*	17.054(3)
51	123	0.030	Cal 100	-	4.991(2)	=*a*	17.050(3)
52	138	0.025	Cal 100	-	4.996(3)	=*a*	17.060(4)
53	137	0.015	Cal 100	-	4.992(2)	=*a*	17.051(3)
54	122	0.010	Cal 100	-	4.991(2)	=*a*	17.051(3)
55	136	0.005	Cal 100	-	4.995(2)	=*a*	17.060(3)

Note: *—numbers are the same as in Table 1; Mhcal—monohydrocalcite, Cal—calcite, Arg—aragonite, Gth—goethite, Mgt—magnetite; -—not detectable (<3 vol.%); ±—traces (3–10 vol.%); +—small amount (10–30 vol.%); □—significant amount (30–50 vol.%); ■—main phase (>50 vol.%).

Table 4. Phase composition (PXRD data) of precipitates synthesized at 23 °C and UCPs of the main CCCs.

No *	Sample Name (CME)	Me^{2+}/Ca, Solution	Crystalline Phase Composition, %	Amorphous Phase	Unit Cell Parameters, Å		
					a	*b*	*c*
			Me^{2+} = Co				
1	20	0.500	Cal 88 Arg 12	±			
2	21	0.400	Cal 89 Arg 11	±			
3	1	0.300	Cal 88 Arg 12	±			
4	25	0.200	Cal 97 Arg 3	±	4.987(3)	=*a*	17.016(2)
5	26	0.100	Cal 95 Arg 5	-	4.982(3)	=*a*	17.010(3)
			Me^{2+} = Ni				
6	22	1.300	-	■			
7	27	1.100	Arg 100	□	4.966(2)	7.975(4)	5.756(2)
8	2	1.000	Arg 90 Cal 10	□	4.964(2)	7.970(3)	5.752(2)
9	28	0.900	Arg 78 Cal 22	+			
10	23	0.800	Cal 61 Arg 39	+			
11	29	0.600	Cal 91 Arg 9	-	4.986 (3)	=*a*	17.039(4)
			Me^{2+} = Cu				
12	30	1.200	Mlc 88 Arg 12	-			
13	31	0.900	Mlc 65 Arg 35	±			
14	32	0.700	Mlc 47 Cal 38 Arg 15	-			
15	24	0.600	Cal 60 Mlc 34 Arg 6	±			
			Me^{2+} = Fe				
16	111	0.500	Cal 63 Gth 37	±			
17	110	0.400	Cal 83 Gth 17	-			
18	109	0.300	Cal 84 Mgt 16	-			
19	108	0.200	Cal 79 Mgt 21	-			
20	107	0.100	Cal 82 Mgt 18	-			
21	81	0.050	Cal 100	+	4.989(3)	=*a*	17.058(4)
22	80	0.030	Cal 100	+	4.991(3)	=*a*	17.047(4)
23	95	0.025	Cal 100	+	4.986(4)	=*a*	17.048(3)
24	94	0.015	Cal 100	-	4.996(4)	=*a*	17.058(4)
25	79	0.010	Cal 100	-	4.991(4)	=*a*	17.060(4)
26	93	0.005	Cal 100	-	4.992(3)	=*a*	17.052(4)

Note: *—numbers are the same as in Table 2; Mhcal—monohydrocalcite, Cal—calcite, Arg—aragonite, Mlc—malachite, Gth—goethite, Mgt—magnetite. -—not detectable (<3 vol.%); ±—traces (3–10 vol.%); +—small amount (10–30 vol.%); □—significant amount (30–50 vol.%); ■—main phase (>50 vol.%).

Optical and SEM–EDX studies showed that the studied crystalline carbonates predominantly form spherical or dumbbell-like aggregates, while AC forms crusts and shapeless

particles (Figures 1–3). For this reason, samples consisting of 1–2 crystalline phases were predominantly studied by optical microscopy and SEM–EDX.

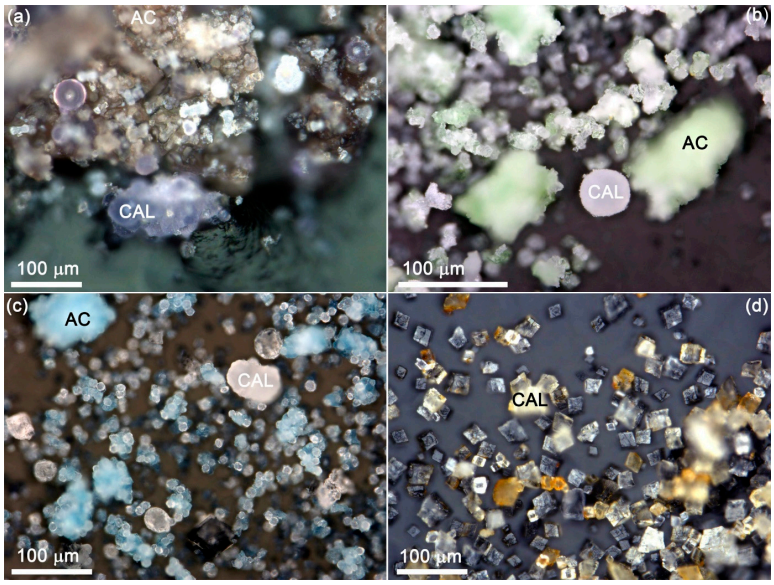

Figure 1. Calcite crystals formed in (**a**) Co-rich solution (sample CAV 42), (**b**) Ni-rich solution (sample CME 29), (**c**) Cu-rich solution (sample CAV 50) and (**d**) Fe-rich solution (sample CME 99). Note: CAL—calcite, AC—amorphous carbonate. Sample numbers (in parentheses) correspond to Tables 1 and 2.

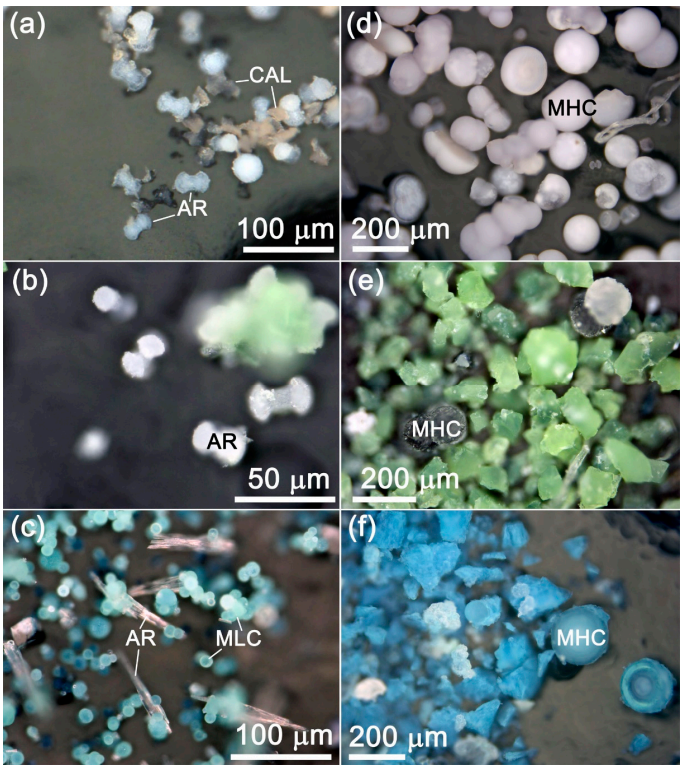

Figure 2. Morphology of synthetic carbonates: (**a**) aragonite, Co-rich solution (CAV 43), (**b**) aragonite, Ni-rich solution (CME 27), (**c**) aragonite, Cu-rich solution (CME 30), (**d**) monohydrocalcite, Co-rich solution (CAV 71), (**e**) monohydrocalcite, Ni-rich solution (CAV 45) and (**f**) monohydrocalcite, Cu-rich solution (CAV 63). Note: MHC—monohydrocalcite, AR—aragonite, CAL—calcite, MLC—malachite. Sample numbers (in parentheses) correspond to Tables 1 and 2.

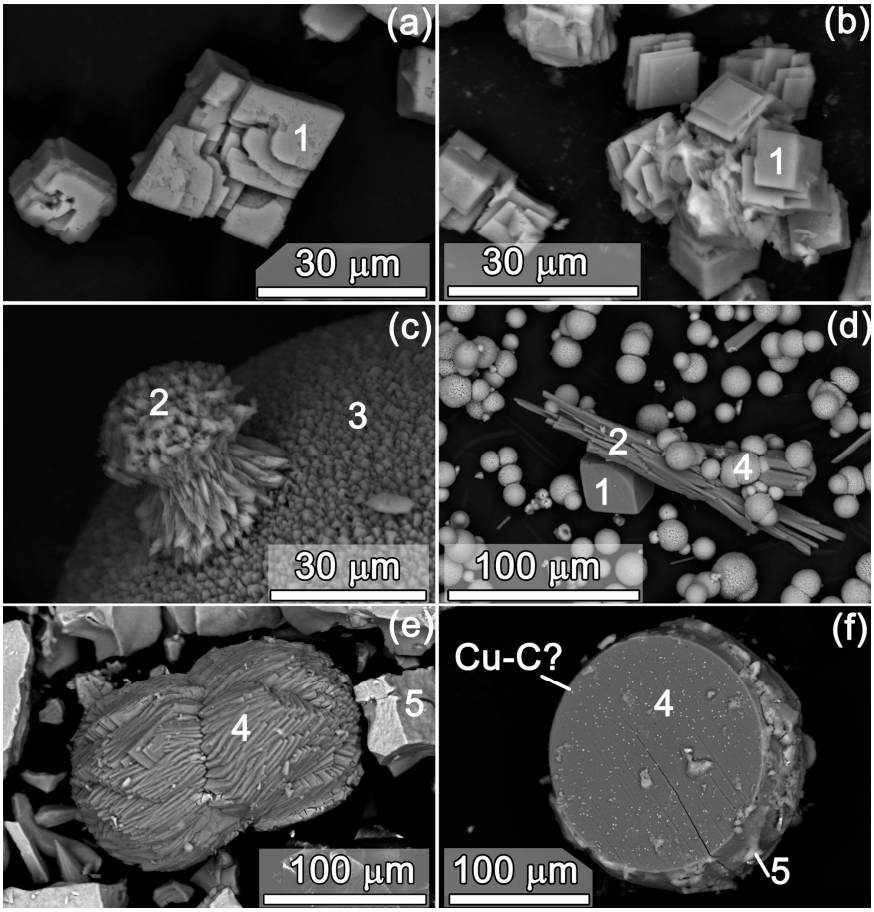

Figure 3. Morphology of synthetic carbonates: (**a**) calcite, Fe-rich solution (CME 93), (**b**) calcite, Co-rich solution (CAV 26), (**c**) aragonite on monohydrocalcite, Co-rich solution (CAV 71), (**d**) malachite on aragonite, Cu-rich solution (CME 30), (**e**) monohydrocalcite and amorphous carbonate, Ni-rich solution (CAV 45), (**f**) amorphous carbonate and malachite on monohydrocalcite, Cu-rich solution (CAV 63). Note: 1—calcite, 2—aragonite, 3—monohydrocalcite, 4—malachite, 5—amorphous carbonate, Cu-C?—Cu-rich carbonate phase (malachite?). Sample numbers (in parentheses) correspond to Tables 1 and 2.

3.1.1. Calcite

Calcite precipitates in Co-, Ni-, Cu- and Fe-rich systems at low (3 °C) and high (23 °C) temperatures (Tables 3 and 4). Its amount can reach 100 vol.% (Tables 3 and 4). This is the most common crystalline carbonate in the studied systems. However, no calcite was found in Co-rich solutions (at low temperature; Table 3) at Co^{2+}/Ca ratio 0.10–0.12 and $pH_{initial}$ 8.50–10.03 (Tables 1 and 3). No calcite was found in Ni-rich solutions (both at low and ambient temperatures; Tables 3 and 4) at Ni^{2+}/Ca ratio 1.10–1.60 and $pH_{initial}$ 7.55–8.18 (Tables 1 and 3). No calcite was found in Cu-rich solutions (both at low and ambient temperatures; Table 3) at Cu^{2+}/Ca ratio 0.90–1.50 and $pH_{initial}$ 5.44–6.93 (Tables 1 and 3).

Calcite forms rhombohedral crystals (Co-, Cu- and Fe-rich systems), spheres (Co-rich systems) and dumbbell-like aggregates (Cu- and Ni-rich systems) up to 50 µm in size (Figure 1a–d, Figures 2a and 3a,b). The shape of calcite crystals clearly depends on temperature, as calcite crystals growing at 3 °C tend to form spheres (CAV 42 and 53; Figure 1a), whereas, at 23 °C, rhombohedral crystals were found (CAV 26; Figure 3a). Calcite is typically covered with AC.

3.1.2. Aragonite

Aragonite precipitates in Co-, Ni- and Cu-bearing systems at low (3 °C) and ambient (23 °C) temperatures (Tables 3 and 4). Its amount can reach 100 vol.% (Tables 3 and 4). No

aragonite was found in Fe-rich solutions (both at low and ambient temperatures; Tables 3 and 4). In Co-rich systems (both at low and ambient temperatures), aragonite forms at Co^{2+}/Ca ratio 0.05–1.00 (all ranges) and $pH_{initial}$ 7.50–10.45 (all ranges) (Tables 1 and 3). In Ni-rich systems (both at low and ambient temperatures), aragonite forms at Ni^{2+}/Ca ratio 0.60–1.20 and $pH_{initial}$ 7.94–9.34. In Cu-rich systems (both at low and ambient temperatures), aragonite forms at Cu^{2+}/Ca ratio 0.60–1.20 and $pH_{initial}$ 6.27–8.72.

Aragonite forms dumbbell-like aggregates (in Co- and Ni-rich systems; Figure 2a,b) and needles (in Cu-rich systems; Figure 2d) up to 100 μm in size (Figures 2a–d and 3c,d). Aragonite aggregates are always transparent and translucent under optical observation (Figure 2a–d). Aragonite is typically covered with AC (Co-/Ni-rich systems)/malachite (Cu-rich systems) and can overgrow calcite (Figure 3c,d).

3.1.3. Monohydrocalcite

Monohydrocalcite precipitates in Co-, Ni- and Cu-rich systems at low temperature (3 °C) only (Table 3). Its amount can reach 100 vol.% (Table 3). No monohydrocalcite was found at ambient temperature (23 °C) synthesis or in Fe-rich solutions (both at low and ambient temperatures; Tables 3 and 4). In Co-rich systems, monohydrocalcite forms at Co^{2+}/Ca ratio (solution) 0.08–0.12 and $pH_{initial}$ 8.77–9.73 (Tables 1 and 3). In Ni-rich systems, monohydrocalcite forms at Ni^{2+}/Ca ratio 0.50–1.00 and $pH_{initial}$ 8.75–8.80. In Cu-rich systems, monohydrocalcite forms at Cu^{2+}/Ca ratio 0.50–1.00 and $pH_{initial}$ 6.56–7.50.

Monohydrocalcite forms spheres up to 200 μm in size (Figures 2d–f and 3e,f), which are composed of stepped twisted crystals (Ni-rich systems; Figure 3a) or thin cone-shaped fibers (50–100 nanometers in size) tightly adjacent to each other (Co- and Cu-rich systems; Figure 3c). Monohydrocalcite aggregates are pinkish (Co-rich systems), colorless (Ni-rich systems) or bluish (Cu-rich systems) (Figure 3c,d) and translucent under optical observation with a distinct opal tint. Monohydrocalcite is typically covered with AC (Figure 2d–f) and overgrown by aragonite (Figure 3c).

3.1.4. Amorphous Carbonate (AC)

Even though crystalline carbonates were the main focus of the current work, it was not possible to achieve completely crystalline samples (e.g., CAV 57, 58, Table 3; CME 22, Table 4). AC forms in all systems at low (3 °C) and ambient (23 °C) temperatures at very early stages of synthesis (aging time < 20 days) but can remain "stable" for a long time (Tables 3 and 4). According to optical observations, the milky solution at the bottom of the beaker was free of crystalline phases for up to ~30–150 days, depending on conditions. Generally, this solution remains "stable" longer at low temperatures. However, in Fe-rich systems, this process lasted ~110 days, even at 23 °C (e.g., No. 16, Table 4). AC is almost constantly present in the resulting precipitates and forms shapeless crusts, which contain CCCs (e.g., Figures 2a and 3a) or small (<<1 μm) particles on the surface of CCCs.

3.1.5. Malachite

Malachite precipitates in Cu-rich systems only (both at low (3 °C) and ambient (23 °C) temperatures; Tables 3 and 4). Its amount can reach 100 vol.% (Table 3). Malachite appears only in the solution withhigh Cu/Ca ratio. No malachite was found at Cu^{2+}/Ca ratio 0.20–0.85 and $pH_{initial}$ 6.80–7.55 (Tables 1 and 3). Malachite forms spheres up to 20 μm in size (Figures 2c and 3d), which are composed of thin fibers (<50 nanometers in size). Malachite aggregates are greenish and translucent under optical observation (Figure 1c). Malachite forms at late stages and typically overgrows aragonite (Figures 1c and 3d).

3.1.6. Iron (Hydro)oxides

Crystalline iron (hydro)oxides (goethite and magnetite) were found in Fe-rich systems, both at low (3 °C) and ambient (23 °C) temperatures (Tables 3 and 4). Generally, goethite forms at higher Fe content (Fe/Ca 0.4–0.5) compared to magnetite (Fe/Ca 0.1–0.3). Optical observations, along with SEM studies, indicate the presence of amorphous iron

(hydro)oxides in syntheses conducted at low Fe content (Fe/Ca < 0.1), as no crystalline phases were detected by PXRD, and the studied calcite crystals were typically covered by a thin orange to yellow crust (Figure 2d).

3.2. Unit Cell Parameters and Chemical Composition of Synthesized Calcium Carbonates

Calcite, aragonite and monohydrocalcite were synthesized as single phases (90–100%; Tables 3 and 4; Figure 4a) at different Me^{2+}/Ca ratios in solution (Tables 3 and 4). All heavy metals (Me^{2+} = Co, Ni, Cu, Fe) have smaller ionic radii than calcium, both in 8- and 6-coordinated polyhedra ($^{VIII}Ca^{2+}$ 1.12 > $^{VIII}Fe^{2+}$ 0.92 > $^{VIII}Co^{2+}$ 0.90 Å; $^{VI}Ca^{2+}$ 1.00 > $^{VI}Fe^{2+}$ 0.78 > $^{VI}Co^{2+}$ 0.745 > $^{VI}Cu^{2+}$ 0.73 > $^{VI}Ni^{2+}$ 0.69 Å; [41]). This means that unit cell parameters of CCCs should (1) decrease as their Me^{2+} content increases and (2) be smaller than that of Me^{2+}-free CCCs.

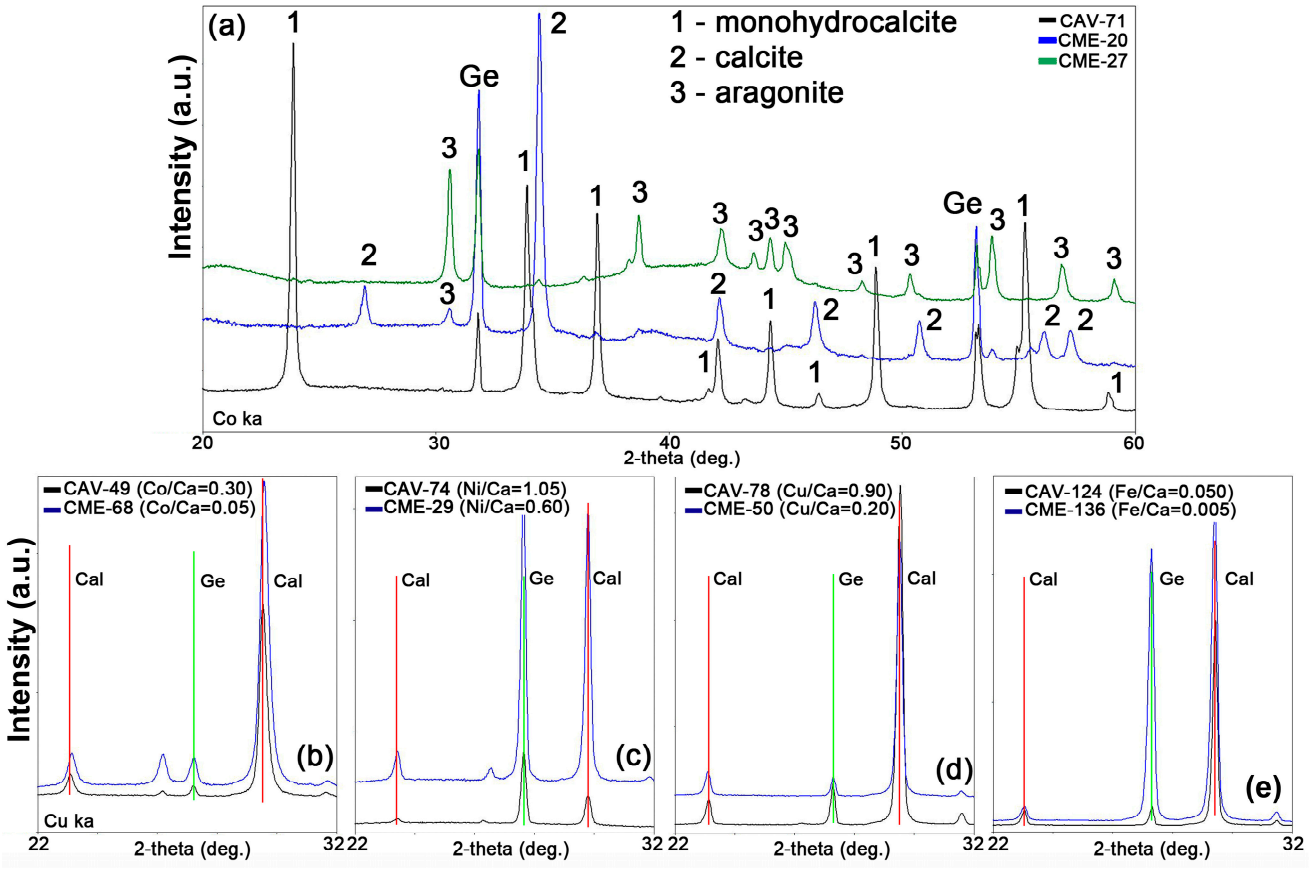

Figure 4. Representative room-temperature PXRD patterns: (**a**) calcite (CME-27), aragonite (CAV 20) and monohydrocalcite (CAV 71), (**b**) calcite precipitated from Co-bearing solutions (CME-68 and CAV-49, respectively), (**c**) calcite precipitated from Ni-bearing solutions (CME-29 and CAV 74, respectively), (**d**) calcite precipitated from Cu-bearing solutions (CME-50 and CAV 78, respectively) and (**e**) calcite precipitated from Fe-bearing solutions (CME-136 and CAV 124, respectively). Note: Cal—calcite, Ge—germanium.

Unfortunately, it was not possible to directly compare UCP values with the content of Me^{2+} in respective phases, as SEM–EDX indicated the studied phases, in most cases, form spheres/dumbbell-like aggregates and often contain impurities located near the crystals of the main phase. Because of this, only semi-quantitative data on their chemical composition were obtained, and data on the Me^{2+}/Ca ratio in solution were used as a proxy of maximum Me^{2+} content in crystalline phases. We also suppose that Me^{2+} maximum concentrations in the studied CCCs are close to the maximum possible content of heavy metals (under given

conditions). It is important to note that the metal may not be incorporated into the lattice but may be sorbed on the surface of CCCs.

3.2.1. Calcite

UCPs of calcite precipitated from Co-(7 syntheses, Co/Ca = 0.050–0.300), Ni- (5 syntheses, Ni/Ca = 0.500–1.050), Cu- (5 syntheses, Cu/Ca = 0.200–0.900) and Fe-rich solutions (13 syntheses, Fe/Ca = 0.100–0.005) were obtained (Tables 3–5). UCPs of synthetic Me^{2+}-free calcite are *a* 4.9900(5), *c* 17.061(3) [42].

The values of *a* and *c* parameters change significantly (over three standard errors) within a Co-rich calcite series. UCPs of calcite precipitated from Co-rich solutions (CAV 46, 49, 52, 53, 67) vary: *a* 4.960(3)–4.970(3), *c* 16.876(3)–17.016(3) Å (Table 3). Intense changes in peak position depending on Co^{2+}/Ca ratio (Figure 4b) and small UCPs (compared to synthetic Me^{2+}-free calcite; Figure 5a) clearly indicate Co incorporation into the calcite crystal lattice (Figure 5b). However, it should be noted that temperature significantly affects this process, as measured Co content in calcite does not directly depend on the Co/Ca ratio in solution (see below).

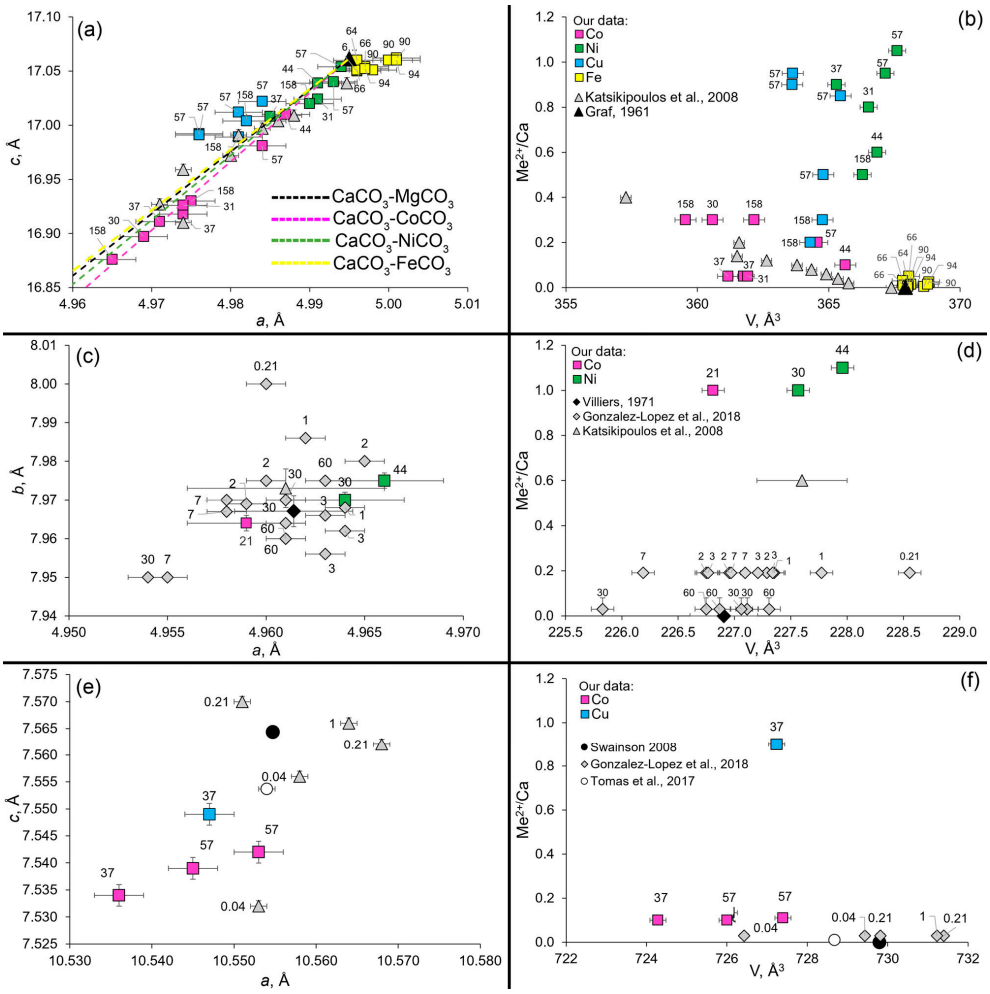

Figure 5. Unit cell parameter variation in calcite (**a**,**b**), aragonite (**c**,**d**) and monohydrocalcite (**e**,**f**) precipitated from Me^{2+}-bearing solutions (Me^{2+} = Co, Ni, Cu, Fe) in comparison with published data [29,30,42–45]: (**a**) *a* vs. *c* in calcite, (**b**) Me^{2+}/Ca vs. unit cell volume of calcite, (**c**) *a* vs. *b* in aragonite, (**d**) Me^{2+}/Ca vs. unit cell volume of aragonite, (**e**) *a* vs. *c* in monohydrocalcite and (**f**) Me^{2+}/Ca vs. unit cell volume of monohydrocalcite. Note: Numbers are aging time (in days).

Only the value of *c* parameter changes significantly (over three standard errors) within the Ni- and Cu-rich calcite series (Figure 5a). The UCPs of calcite precipitated from Ni-rich

solutions (CAV 29, 51. 74–76) vary: *a* 4.985(3)–4.989(3), *c* 17.008(3)–17.054(4) Å (Table 3). The UCPs of calcite precipitated from Cu-rich solutions (CAV 44, 47, 50, 78–79) vary: *a* 4.971(3)–4.979(3), *c* 16.989(3)–17.022(4) Å (Table 3). The position of the calcite peaks weakly depends on the content of Ni/Cu in the solution (Figure 4c,d). However, the UCPs of synthetic calcite precipitated in a Ni-/Cu-rich system are always slightly smaller (especially *c* parameter) than the UCPs of synthetic Me^{2+}-free calcite (Figure 5a,b), which indicates possible Ni/Cu incorporation into the calcite.

The values of *a* and *c* UCPs change significantly (over three standard errors) within the Fe-rich calcite series (Figure 5a,b). The UCPs of calcite precipitated from Fe-rich solutions (CAV 122–124, 137–138, 150; CME 79–81, 93–95) vary: *a* 4.986(3)–4.996(3), *c* 17.047(3)–17.060(4) Å (Table 3). Interestingly, only cell parameters of calcites synthesized at different temperatures differ, but no changes in calcite peak position depending on Fe^{2+}/Ca ratio were found on the X-ray diagram (Figure 4e). The UCPs of synthetic calcite precipitated at 3 °C in Fe-rich solutions (Table 3) are the same as for synthetic Me^{2+}-free calcite, while the UCPs of synthetic calcite precipitated at 23 °C in Fe-rich solutions are slightly smaller than those of synthetic Me^{2+}-free calcite (Figure 5a). This indicates possible Fe incorporation (in very small amounts) into the calcite crystal lattice at 23 °C.

The points corresponding to calcites with cobalt and nickel impurities fit into the dependencies for the series $CaCO_3$-$CoCO_3$ and $CaCO_3$-$NiCO_3$, respectively (Figure 5a). The UCPs of calcites synthesized in the presence of copper fit into a different trend, which may indicate the possibility of the existence of a copper-enriched carbonate with a calcite structure.

SEM–EDX showed that calcite precipitated from Co-rich solutions can contain up to ~13.0 wt.% CoO and up to ~1.0 wt.% Na_2O (CAV 42; Co/Ca = 0.50). It is worth noting that a cobalt content increase in the solution of 10 times leads to an increase in the content of cobalt in calcite only by a factor of two (~13.0 wt.% and ~7.0 wt.% CoO; Co/Ca = 0.50 and 0.05, CAV 42 and CAV 53, respectively). Temperature significantly affects this process. Well-shaped (rhombohedral) calcite precipitated at higher Co/Ca (CAV 26, Co/Ca 0.10) and 23 °C contains less Co (2–4 wt.% CoO) compared to sphere-like calcite precipitated at lower Co/Ca (CAV 53, Co/Ca 0.05) and 3 °C (6–7 wt.% CoO). These data are in good agreement with UCPs and support Co incorporation into the calcite crystal lattice.

SEM–EDX showed that calcite precipitated from a Ni-rich solution can contain up to ~3.0 wt.% NiO (CAV 74; Ni/Ca = 1.050) and from a Cu-rich solution—up to ~4.0 wt.% CuO (CME 77 Cu/Ca = 0.95). No iron was found in calcite precipitated from Fe-rich solutions. No relation between Ni/Cu content in calcite and Cu/Ni/Ca ratio in solution/temperature/time of exposure was found.

3.2.2. Aragonite

The UCPs of aragonite precipitated from Co-rich solution (Co/Ca = 1.00) after 21 days of exposure (CAV 43) are *a* 4.959(2), *b* 7.964(3), *c* 5.743(2) Å (Table 3; Figure 5c). The UCPs of aragonite precipitated from Ni-rich solutions (two syntheses, CAV 2, 7; Ni/Ca = 1.00–1.10, exposure time 30–44 days) are almost identical (*a* 4.964–4.966(2), *b* 7.970(3)–7.975(4), *c* 5.752(2)–5.756(2) Å (Table 3; Figure 5c)). However, these values (aragonite UCPs in Co- and Ni-rich systems) can be considered very close since the difference between them is within three standard errors. The UCPs of natural Me^{2+}-free aragonite ($Ca_{0.997}Sr_{0.0021}Mg_{0.004}Pb_{0.0005}CO_3$; 4.9614(3), 7.9671(4), 5.7404 (4) Å; [43]) are almost identical to our synthetic aragonite (except *c* parameter). We can conclude that neither Ni nor Co could be incorporated into aragonite and be reliably detected using the applied approach (Figure 5d).

SEM–EDX showed that aragonite precipitated from Co-rich solutions can contain up to ~3.0 wt.% CoO (CAV 43; Co/Ca = 1.00), from Cu-rich solution—up to ~3.0 wt.% CuO (CME 30; Cu/Ca = 1.20) and from Ni-rich solution—up to ~3.0 wt.% NiO (CME 27; Ni/Ca = 1.10). However, we cannot fully rely on these values, as individual crystals (<1 μm) are smaller than the typical EDX spot.

3.2.3. Monohydrocalcite

The UCPs of monohydrocalcite precipitated from Co-bearing solutions (three syntheses, CAV 70–72, Co/Ca = 0.10–0.11) vary: *a* 10.536(4)–10.553(3), *c* 7.534(2)–7.542(2) Å (Table 3; Figure 5e). It is worth noting that these syntheses were stopped at different times (after 37 (CAV 70) and 57 days (CAV 71 and CAV 72; Table 1)). Monohydrocalcites precipitated after 57 days (CAV 71 and CAV 72) have the same UCPs, while the one stopped at earlier stages (CAV 70) has considerably smaller values (Figure 5e). The established difference in the cell parameters within the cobalt series significantly exceeds three standard errors, which indicates significant changes in the lattice metric. Unit cell parameters of monohydrocalcite precipitated from a Cu-rich solution (Ni/Ca = 0.90) after 37 days of exposure (CAV 63) are *a* 10.547(4), *c* 7.549(2) Å. The UCPs of natural Me^{2+}-free monohydrocalcite (*a* 10.5547(4), *c* 7.56440(29) Å, Ref. [44]) are significantly greater than those of our synthetic monohydrocalcites (Figure 5e). We can conclude that Co and Cu can be incorporated into monohydrocalcite crystal lattices, and exposure time has a great influence on this process.

SEM–EDX showed that monohydrocalcite precipitated from Co-rich solutions can contain up to ~1.0 wt.% CoO (CAV 71; Co/Cab = 0.11), from Cu-rich solutions—up to ~2.0 wt.% CuO (CAV 45; Cu/Ca = 1.00) and from Ni-rich solutions—up to ~3.0 wt.% NiO (CAV 63; Ni/Ca = 0.90). We did not observe chemical zoning or any other variation in chemical composition of monohydrocalcite within a sample.

3.2.4. Amorphous Carbonate

Amorphous carbonate can contain up to ~50 wt.% CoO/~40 wt.% NiO/~60 wt.% CuO. It is also Cl-bearing (0.5–2.0 wt.% Cl) and possibly sufficiently hydrated, which is indicated by low EDX totals (<~65 wt.%) and significant surface cracking during SEM–EDX studies.

4. Discussion

4.1. The Effect of Temperature

Temperature significantly influenced crystallization pathways and the resulting phase composition. No $CoCO_3$ (synthetic analogue of spherocobaltite, calcite structure type), $NiCO_3$ (synthetic analogue of gaspéite, calcite structure type), $CuCO_3$ (no mineral known, unique structure) or $FeCO_3$ (synthetic analogue of siderite, calcite structure type) were synthesized, despite relatively high Me^{2+} content in the mother solution (Tables 1, 2 and 5).

Spherocobaltite occurs all over the world [46] and is widely synthesized for technical purposes (e.g., [47]). Previously, it was found that the reaction temperature (typically >> 100 °C [47,48]) is a key factor in the formation of the $CoCO_3$ crystals, as the reaction rate decreases with the reaction temperature decreasing, thus decreasing the nucleation rate and growth rate (e.g., [49]). So, probably no spherocobaltite can be obtained at low (<30 °C) temperatures. Gaspéite quite rarely occurs in nature (e.g., [50]), probably due to its instability in air conditions (e.g., [51]). It was successfully synthesized using a hydrothermal technique (e.g., [48]). However, high temperature (>100 °C [52]) is also favored for its formation. $CuCO_3$ was found to be formed at high pressure–temperature (PT) conditions only (20 kbar, 500 °C [53]) and has not been found in nature so far. Siderite is a quite common mineral and can be synthesized at various temperatures (15–360 °C, e.g., [36,54]) at aging time <1 day (e.g., [54]). However, a high Fe/dissolved inorganic carbon ratio is needed (>0.003 [54]), which was not the case in our experiments (Tables 3 and 4). We can conclude that temperature could be the main factor controlling the presence of $CoCO_3/NiCO_3/CuCO_3$ in resulting precipitates.

Another striking example of temperature-controlled phase composition is monohydrocalcite, which can precipitate from Co-/Ni-/Cu-rich solutions at 3 °C only (Table 3). Previously, no data on synthetic monohydrocalcite obtained in a Cu/Ni system were available, but monohydrocalcite was synthesized in a Co-rich solution at 25 °C as an intermediate phase (1–24 h) and dissoluted after 1 day of aging [30]. Additionally, natural monohydrocalcite with high Cu content ($(Ca_{0.99}Cu_{0.01})CO_3 \cdot H_2O$ [45]) was found in the Špania Dolina (Slovakia) deposit. This sample most likely also crystallized at lower

temperatures, as it was found in underground tunnels [45]. Previous studies of a Ca–Mg–CO_3–H_2O system at 3 and 23 °C also showed higher abundancy of monohydrocalcite at low temperatures [22]. We can conclude that monohydrocalcite can be formed as an intermediate metastable phase in Co-/Ni-/Cu-/Mg-rich systems but remains stable (>100 days) if precipitated at low temperatures in Co-/Ni-/Cu-rich systems.

Our data indicate that aragonite content tends to increase as temperature increases in Ni-/Cu-rich systems. Comparison of syntheses provided almost the same *Me*/Ca ratio (e.g., CAV 63 and CME 31/CAV 66 and CME 27, Ni/Ca 1.10 and Cu/Ca 0.90, respectively; Tables 3 and 4) and aging time (37 (CAV 63 and 66) and 44 days (CME 31 and 31 and 27); Tables 1 and 2) and showed the content of aragonite increases by a third (from 0 to 35% and from 66 to 100%, respectively) with increasing temperature from 3 to 23 °C. Data on Co-rich systems do not contradict these findings (Tables 3 and 4), but wide variations in pH significantly complicate the observed tendencies. This process is the result of (1) monohydrocalcite—aragonite transformation (due to monohydrocalcite instability at higher temperatures) and (2) calcite instability in Me^{2+}-rich systems.

4.2. The Effect of Aging Time

Our data show that aging time (exposure time in solution) significantly influences the resulting phase composition. Syntheses performed at the same conditions (Me^{2+}/Ca ratio, Ca/CO_3 ratio, pH) but stopped at different stages show completely different phase compositions (Tables 3 and 4). It seems that the studied systems do not achieve thermodynamic stability, even after ~100 days of aging, as monohydrocalcite, aragonite and amorphous carbonate were present in the resulting precipitate.

Monohydrocalcite is thought to be a metastable phase, but its content could increase as aging time increases. Monohydrocalcite becomes the main phase when the exposure time is doubled in Co-rich systems (CAV 56: Co/Ca 1.4, $pH_{initial}$ 9.61, aging time 31 days, calcite 66%, aragonite 34%; CAV 72: Co/Ca 1.4, $pH_{initial}$ 9.73, aging time 57 days, monohydrocalcite 100%; Table 3). However, an inverse relationship was also found: monohydrocalcite content decreases dramatically when the exposure time is doubled in Ni-rich systems (CAV 45: Ni/Ca 1.0, $pH_{initial}$ 8.75, aging time 57 days, monohydrocalcite 64%, calcite 36%; CAV 98: Ni/Ca 1.0, $pH_{initial}$ 8.85, aging time 114 days, calcite 85%, monohydrocalcite 15%; Table 3). Generally, the same tendency was observed in Cu-rich systems (CAV 63: Cu/Ca 0.9, $pH_{initial}$ 6.93, aging time 37 days, monohydrocalcite 100%; CAV 78: Cu/Ca 0.9, $pH_{initial}$ 6.75, aging time 57 days, calcite 96%, aragonite 4%; Table 3).

Amorphous carbonate with high Me^{2+} content (up to 60 wt.% *Me*O) is always present in the first stage of synthesis and can remain stable for ~100 days (Tables 3 and 4). We think that long-term studies (aging time > 1 year) and computer simulations are needed to establish whether it is possible to completely transform amorphous carbonate into crystalline phases (under given conditions) or whether it is (thermodynamically?) limited.

4.3. Heavy Metal (Me^{2+} = Co, Ni, Cu, Fe) Incorporation into CCC Lattices

Some of the heavy metals under consideration may enter the CCC lattices in sufficient amounts (e.g., Co), while the entry of others is limited (e.g., Cu, Ni) or almost impossible (e.g., Fe). The type of cation and the peculiarity of the CCC crystal structure are the main limiting factors.

Calcite can host Co in sufficient amounts. Our data show that calcite unit cell volume decreases from ~366 to ~359 $Å^3$ (our data) while Co/Ca in solution increases (Table 5; Figure 5b). This is in good agreement with Katsikopoulos et al. [29], who showed that calcite unit cell volume decreases from 369 to 362 $Å^3$ while Co/Ca in solution increases. These data also indicate that low temperatures are favorable for Co incorporation into calcite crystal lattices. It is worth noting that Me^{2+}-free calcite has considerably higher unit cell volume (368 $Å^3$ [42]) than that of synthetic Co-bearing calcites, which clearly indicates Co incorporation (Table 5).

Table 5. Comparison of unit cell volumes (V) of CCCs, obtained at different Me/Ca ratios, temperatures and aging times.

No.	Sample Name	*T*, °C	Aging Time, Days	Me^{2+}	Me^{2+}/Ca, Solution	Main Phase	V, Å^3	Ref.	Δ_1, Å^3	Δ_2, Å^3
1	-	natural		-	0.000	Calcite ($CaCO_3$)	367.90(1)	[42]	-	-
2	CAV-49	23	158	Co	0.300		362.2(3)	This study	6.0	8.3
3	CAV-52		158		0.300		359.6(3)			
4	CAV-46		57		0.200		364.6(3)			
5	CAV-67		37		0.050		361.2(3)			
6	CAV-53		31		0.050		361.9(3)			
7	CME-25	3	44		0.200		366.5(3)			
8	CME-26		44		0.100		365.6(3)			
9	CAV-74	23	57	Ni	1.050		367.6(3)		1.3	1.6
10	CAV-76		57		0.950		367.2(3)			
11	CAV-51		158		0.500		366.3(3)			
12	CME-29	3	44		0.600		366.8(3)			
13	CAV-78	23	57	Cu	0.900		363.6(3)		1.8	4.3
14	CAV-79		57		0.850		365.4(3)			
15	CAV-44		57		0.500		364.8(3)			
16	CAV-47		158		0.300		364.8(3)			
17	CAV-50		158		0.200		364.3(3)			
18	CAV-150		44	Fe	0.100		368.6(3)		1.8	0.9
19	CAV-124		66		0.050		368.0(3)			
20	CAV-123		66		0.030		367.8(3)			
21	CAV-138		90		0.025		368.8(3)			
22	CAV-137		90		0.015		368.1(3)			
23	CAV-122		66		0.010		367.8(3)			
24	CAV-136		90		0.005		368.6(3)			
25	CME-81	3	64	Fe	0.050		367.8(3)			
26	CME-80		64		0.030		368.2(3)			
27	CME-95		94		0.025		367.0(3)			
28	CME-94		94		0.015		368.8(3)			
29	CME-79		64		0.010		368.0(3)			
30	CME-93		94		0.005		368.0(3)			
31	-	~222	2	Co	-	Spherocobaltite ($CoCO_3$)	281.62(1)	[48]	-	86.3
32	-	~222	2	Ni	-	Gaspéite ($NiCO_3$)	271.39(1)		-	96.5
33	-	-	-	Fe	-	Siderite ($FeCO_3$)	293.17	[8]	-	74.7
34	-	natural		-	-	Aragonite ($CaCO_3$)	226.91(1)	[43]	-	-
35	CAV-43	23	21	Co	1.000		226.8(3)	This study	1.2	1.1
36	CME-27	3	44	Ni	1.100		228.0(3)			
37	CME-2		30	Ni	1.000		227.6(3)			

Table 5. *Cont.*

No.	Sample Name	*T*, °C	Aging Time, Days	Me^{2+}	Me^{2+}/Ca, Solution	Main Phase	V, Å^3	Ref.	Δ_1, Å^3	Δ_2, Å^3
38	-		natural	-	-		729.79(6)	[44]		
39	-		natural	Cu	-		728.68(18)	[45]		1.11
40	CAV-71		57	Co	0.110	Monohydrocalcite ($CaCO_3 \cdot H_2O$)	727.4(3)			
41	CAV-70	23	37	Co	0.100		724.3(3)	This study	3.1	5.49
42	CAV-72		57	Co	0.100		726.0(3)			
43	CAV-63		37	Cu	0.900		727.2(3)			

Note: $\Delta_1 = V_{max} - V_{min}$, $\Delta_2 = |{}^{me\text{-}free}V - {}^{synth}V_{min}|$.

Our data indicate limited solubility of $CoCO_3$ in $CaCO_3$ (both at 3 and 23 °C), as Co content in calcite does not exceed ~0.15–0.25 apfu (<13 wt.% CoO). This is consistent with previous studies by Glynn [55] and Katsikopoulos et al. [29], who showed that Co incorporation in calcite is limited to ~3–16 mol.%, while Ca incorporation in spherocobaltite is limited to ~5–7 mol.%. Katsikopoulos et al. [29] also confirmed that spherocobaltite does not precipitate directly from aqueous solution at 25 °C (and ambient pressure). Moreover, the results of a computer simulation study of the mixing of calcite and spherocobaltite suggested that experimental-based thermodynamic models significantly overestimate the solubility between the two solids and, therefore, underestimate the extension of the miscibility gap under ambient conditions [56]. Authors also conclude that carbonates of $Ca_{1-x}Co_xCO_3$ solid solutions are metastable with respect to many compositions observed in nature [56].

Calcite can host very small amounts of Ni and Cu. The unit cell volumes of calcites precipitated from Ni-rich solutions (our data) almost do not differ (366–368 Å^3) but are significantly less than that of Me^{2+}-free calcite (368 Å^3, Ref. [42]; Table 5; Figure 5b). It is important that neither Ni content in solution, temperature or aging time influence the UCPs. The unit cell volumes of calcites precipitated from Cu-rich solutions (our data) also vary insignificantly (364–365 Å^3) but are significantly smaller than that of Me^{2+}-free calcite (368 Å^3 [42]). Our observations are consistent with data on natural and synthetic carbonates of $(Ca,Ni)CO_3/(Ni,Ca)CO_3$ and $(Ca,Cu)CO_3/(Cu,Ca)CO_3$ solid solutions (e.g., [55]). Previously, calcites containing 0.83 and 0.65% Ni were reported by Maksimovic [57] and Maksimovic and Stupar [58], while gaspéite can contain up to 0.45 wt.% CaO [50]. Interestingly, previous studies of $NiCO_3$-$MgCO_3$ systems revealed that solid solutions of intermediate compositions, such as Mg-bearing gaspéite, may form metastably at low temperatures, but they are thermodynamically unstable with respect to unmixing [52]. Copper is also not a common impurity for natural calcites (e.g., [59]), and no mineral with $CuCO_3$ composition has been found yet. Thus, we can conclude that a miscibility gap between calcite and $NiCO_3/CuCO_3$ is even bigger than that in the case of spherocobaltite.

Iron incorporation into calcite crystal lattice is doubtful under the studied conditions. The unit cell volumes of calcites precipitated from Fe-rich solutions (our data) vary from ~366 (23 °C) to ~369 (3 °C) and are close to that of Me^{2+}-free calcite (368 Å^3 [42]; Table 5; Figure 5b). Previously, it was shown that the solid solution $(Ca,Fe)CO_3$ is not complete (e.g., [28] and a number of works report a wide miscibility gap also at high temperatures (T > 300 °C; e.g., [60])). Glynn [55] showed that Fe incorporation in calcite is limited to ~3–18 mol.%, while Ca incorporation in siderite is limited to ~23 mol.%. So, one can suggest that the Fe content in the studied calcite should vary significantly. However, very limited data are available on $(Ca,Fe)CO_3/(Fe,Ca)CO_3$ solid solutions at low (<<25 °C) temperature. Our data show that low Fe content (Fe/Ca 0.005–0.025) at low and ambient temperatures (3–23 °C) resulted in the appearance of AC and required a very long time for CCC crystallization. This inhibitory effect induced by ferrous iron on calcite growth was previously mentioned based on growth experiments [28]. Higher Fe content in solution (Fe/Ca 0.1) re-

sulted in the appearance of iron (hydro)oxides, but no Fe-rich calcite/aragonite crystallized (Tables 3 and 4). Previously, it was shown that the aqueous solution becomes supersaturated with respect to siderite at lower concentrations than with respect to calcite as a result of its lower solubility product at 25 °C [61], but precipitation is hindered for kinetic reasons [62].

An aragonite crystal lattice cannot host a significant amount of Co/Ni/Cu, which is evident from UCP data on synthetic Co- (our data, Ref. [30]) and Ni-rich samples and optical/EDX data on Cu-rich samples (our data; Table 5; Figure 5d). Aging time and temperature do not affect the dependencies obtained. The unit cell volume of aragonite precipitated in a Co-rich system at 3 °C is ~226 Å^3 (our data), in a Co-rich system at 25 °C is ~227 Å^3 [30] and in a Ni-rich system at 23 °C is ~227 Å^3 (our data; Figure 5d). These values are indistinguishable from natural Me^{2+}-free aragonite (227 Å^3 [43]). Previously, aragonite was thought to host some Co [29,30], but this synthetic "Co-aragonite" has higher UCPs than the Co-free one [43]; this fact has not yet been clearly explained. Interestingly, aragonite was successfully synthesized in an Fe-rich solution at 25 °C [28], and this aragonite was thought to be Fe-bearing. However, no UCP data were obtained during this study [28].

A monohydrocalcite crystal lattice can host Co, Ni and Cu in small amounts, which is evident from UCP data on synthetic Co- (our data, Ref. [30]), Ni- (our data) and Cu-rich (our data) and naturally Cu-rich samples [45] (Figure 5c,d). The maximum content of Me^{2+} is quite small and probably limited to ~0.1 apfu. It is worth noting that this value is close to that of monohydrocalcite synthesized in an Mg-rich system [22,40].

The amount of Me^{2+} in monohydrocalcite decreases as aging time increases or temperature increases (our data, Ref. [30]). The unit cell volume increases from 724 to 728 Å^3 as aging time increases (from 37 to 57 days) in syntheses carried out at 3 °C (our data). Similarly, the unit cell volume increases from ~725 to ~729/~729 to 733 Å^3 as aging time increases (from 1 to 24 h), based on data on syntheses carried out at 25 °C [30]. The unit cell volume of Me^{2+}-free natural monohydrocalcite is ~730 Å^3, which is significantly higher than the values of most synthetic monohydrocalcites. Probably, low temperature favors Me^{2+} incorporation into monohydrocalcite and stabilizes it.

5. Conclusions

Crystalline calcium carbonates occur worldwide and play an important role in the carbon cycle and heavy metal sorption. The results of syntheses at different Me^{2+}/Ca ratios, temperatures and aging times showed that the presence of heavy metals in the crystallization medium dramatically changes the crystallization pathways and precipitated phase composition at both low (3 °C) and ambient (23 °C) temperatures. Instead of the normal sequence of calcium carbonate (amorphous calcium carbonate (ACC) → vaterite → calcite), aragonite and monohydrocalcite were found to be the main phases in the resulting precipitate from the Co-/Ni-/Cu-rich systems. In contrast, calcium carbonate crystallization was not significantly affected in the Fe-rich systems. It is likely that the complex behavior of Fe ions in aqueous solution is of paramount importance in explaining this pattern. We can suggest that Fe ions stabilize ACC but do not kinetically/thermodynamically influence the crystallization pathways.

Our data indicate that the crystallization temperature and aging time (exposure time in solution) sufficiently affect the final phase composition of precipitates. Low temperature (3 °C) is favorable for monohydrocalcite and amorphous carbonate, while calcite tends to form more frequently at ambient temperature (23 °C). This could be an explanation for monohydrocalcite/aragonite formation in cold-water marine organisms (e.g., [14,39]) and the specific mineralogy of caves (e.g., [45]). High exposure time in solution leads to a decrease in the content of amorphous carbonate and monohydrocalcite. However, monohydrocalcite aged in solution for a long time is a stable phase and does not undergo further decomposition.

Heavy metals can be incorporated into the calcite/monohydrocalcite crystal lattice in sufficient quantities, while aragonite can host very small amounts of Me^{2+} (or none). Their

content decreases with time if monohydrocalcite is aged in the mother solution. Calcite can concentrate sufficient amounts of Co, small amounts of Ni/Cu and almost no Fe.

It is worth noting that amorphous carbonate is the main carrier of heavy metals in the system in question. Despite the fact that heavy metals precipitate from solution (amorphous carbonate forms), we cannot state that they take a completely insoluble form. Further transformations of amorphous carbonate into crystalline phases will inevitably lead to the formation of calcite/aragonite/monohydrocalcite, the structure of which has a very low ability to absorb the cations under consideration. Simultaneously, the formation of $CoCO_3$/$NiCO_3$/$CuCO_3$/$FeCO_3$ seems to be unfavorable under low and ambient temperature conditions.

The results obtained can be used to solve environmental issues and in mineral resource management. Our studies show that crystalline calcium carbonates, in general, concentrate heavy metals quite poorly at ambient and low temperatures. Moreover, the concentrator phases (e.g., monohydrocalcite) are metastable, which can subsequently lead to the release of heavy metals during their recrystallization. It can be proposed to use the obtained results for the temporary binding into carbonate form of a significant part of transition metal cations in natural or industrial waters, with the possibility of further releasing these cations for subsequent use. One possible future direction of research could be to expand the list of cation additives to study the possibility of their extraction from the aquatic environment for the purpose of both water purification and the use of these elements for technical purposes. Further studies of amorphous calcium carbonates enriched in heavy metals are also needed.

Author Contributions: Conceptualization, O.S.V. and O.V.F.-K.; synthesis, M.A.K.; PXRD studies, I.A.C. and O.S.V.; writing—original draft preparation, O.S.V., M.A.K., I.A.C. and O.V.F.-K.; visualization, O.S.V.; funding acquisition, O.V.F.-K. All authors have read and agreed to the published version of the manuscript.

Funding: This research was funded by the Russian Science Foundation, grant number 19-17-00141.

Data Availability Statement: Data available on request.

Acknowledgments: The laboratory research was carried out in the Research Resource Centers of Saint Petersburg State University "Microscopy and microanalysis", "Geomodel" and "X-ray Diffraction Studies".

Conflicts of Interest: The authors declare no conflict of interest.

References

1. Summerfield, M.A. *Global Geomorphology: An Introduction to the Study of Landforms*; Longman Sc.: New York, NY, USA, 1991.
2. Sulpis, O.; Jeansson, E.; Dinauer, A.; Lauvset, S.K.; Middelburg, J.J. Calcium Carbonate Dissolution Patterns in the Ocean. *Nat. Geosci.* **2021**, *14*, 423–428. [CrossRef]
3. Lowenstam, H.A.; Weiner, S. *On Biomineralization*; Oxford University Press: New York, NY, USA, 1989.
4. Bindschedler, S.; Cailleau, G.; Verrecchia, E. Role of Fungi in the Biomineralization of Calcite. *Minerals* **2016**, *6*, 41. [CrossRef]
5. Millero, F.J.; Woosey, R.; Ditrolio, B.; Water, J. Effect of Ocean Acidification on the Speciation of Metals in Seawater. *Oceanography* **2009**, *22*, 72–85. [CrossRef]
6. Stumm, W.; Morgan, J.J. *Aquatic Chemistry: Chemical Equilibria and Rates in Natural Waters*; John Wiley & Sons: Hoboken, NJ, USA, 2012.
7. Falini, G.; Fermani, S.; Gazzano, M.; Ripamonti, A. Structure and Morphology of Synthetic Magnesium Calcite. *J. Mater. Chem.* **1998**, *8*, 1061–1065. [CrossRef]
8. Effenberger, H. Crystal Structure and Infrared Absorption Spectrum of Synthetic Monohydrocalcite, $CaCO_3$ H_2O. *Monatshefte Für Chem.* **1981**, *112*, 899–909. [CrossRef]
9. Caspi, E.N.; Pokroy, B.; Lee, P.L.; Quintana, J.P.; Zolotoyabko, E. On the Structure of Aragonite. *Acta Crystallogr. Sect. B Struct. Sci.* **2005**, *61*, 129–132. [CrossRef] [PubMed]
10. Boettcher, A.L.; Wyllie, P.J. The Calcite-Aragonite Transition Measured in the System CaO-CO_2-H_2O. *J. Geol.* **1968**, *3*, 314–330. [CrossRef]
11. Garvie, L.A.J. Seasonal Formation of Ikaite in Slime Flux Jelly on an Infected Tree (Populus fremontii) Wound from the Sonoran Desert. *Sci. Nat.* **2022**, *109*, 48. [CrossRef]
12. Rodriguez-Navarro, C.; Kudłacz, K.; Cizer, Ö.; Ruiz-Agudo, E. Formation of Amorphous Calcium Carbonate and Its Transformation into Mesostructured Calcite. *CrystEngComm* **2015**, *17*, 58–72. [CrossRef]
13. Ontl, T.A.; Schulte, L.A. Soil Carbon Storage. *Nat. Educ. Knowl.* **2012**, *3*, 35.

14. Little, S.H.; Wilson, D.J.; Rehkämper, M.; Adkins, J.F.; Robinson, L.F.; van de Flierdt, T. Cold-Water Corals as Archives of Seawater Zn and Cu Isotopes. *Chem. Geol.* **2021**, *578*, 120304. [CrossRef]
15. Défarge, C. Organomineralization. In *Encyclopedia of Geobiology*; Reitner, J., Thiel, V., Eds.; Springer: Dodrecht, The Netherlands, 2011; pp. 697–701.
16. Sondi, I.; Mikac, N.; Vdović, N.; Ivanić, M.; Furdek, M.; Škapin, S.D. Geochemistry of Recent Aragonite-Rich Sediments in Mediterranean Karstic Marine Lakes: Trace Elements as Pollution and Palaeoredox Proxies and Indicators of Authigenic Mineral Formation. *Chemosphere* **2017**, *168*, 786–797. [CrossRef] [PubMed]
17. de Nooijer, L.J.; Reichart, G.J.; Duenas-Bohorquez, A.; Wolthers, M.; Ernst, S.R.; Mason, P.R.D.; van der Zwaan, G.J. Copper Incorporation in Foraminiferal Calcite: Results from Culturing Experiments. *Biogeosciences* **2007**, *4*, 493–504. [CrossRef]
18. Raiswell, R.; Brimblecombe, P. The Partition of Manganese into Aragonite between 30 and 60 °C. *Chem. Geol.* **1977**, *19*, 145–151. [CrossRef]
19. Mavromatis, V.; Goetschl, K.E.; Grengg, C.; Konrad, F.; Purgstaller, B.; Dietzel, M. Barium Partitioning in Calcite and Aragonite as a Function of Growth Rate. *Geochim. Cosmochim. Acta* **2018**, *237*, 65–78. [CrossRef]
20. Brazier, J.M.; Mavromatis, V. Effect of Growth Rate on Nickel and Cobalt Incorporation in Aragonite. *Chem. Geol.* **2022**, *600*, 120863. [CrossRef]
21. Gutjahr, A.; Dabringhaus, H.; Lacmann, R. Studies of the Growth and Dissolution Kinetics of the $CaCO_3$ Polymorphs Calcite and Aragonite II. The Influence of Divalent Cation Additives on the Growth and Dissolution Rates. *J. Cryst. Growth* **1996**, *158*, 310–315. [CrossRef]
22. Vereshchagin, O.S.; Frank-Kamenetskaya, O.V.; Kuz'mina, M.A.; Chernyshova, I.A.; Shilovskikh, V.V. Effect of Magnesium on Monohydrocalcite Formation and Unit-Cell Parameters. *Am. Mineral.* **2021**, *106*, 1294–1305. [CrossRef]
23. Li, Y.; Zhou, Q.; Ren, B.; Luo, J.; Yuan, J.; Ding, X.; Bian, H.; Yao, X. Trends and Health Risks of Dissolved Heavy Metal Pollution in Global River and Lake Water from 1970 to 2017. In *Reviews of Environmental Contamination and Toxicology*; Springer: Cham, Switzerland, 2020; Volume 251, pp. 1–24.
24. Liao, Z.; Wu, S.; Zhang, H.; Chen, F. Removal of Aqueous Cu^{2+} by Amorphous Calcium Carbonate: Efficiency and Mechanism. *Minerals* **2022**, *12*, 362. [CrossRef]
25. Macomber, L.; Hausinger, R.P. Mechanisms of Nickel Toxicity in Microorganisms. *Metallomics* **2011**, *3*, 1153–1162. [CrossRef]
26. Leyssens, L.; Vinck, B.; Van Der Straeten, C.; Wuyts, F.; Maes, L. Cobalt Toxicity in Humans—A Review of the Potential Sources and Systemic Health Effects. *Toxicology* **2017**, *387*, 43–56. [CrossRef]
27. Sun, Z.; Gong, C.; Ren, J.; Zhang, X.; Wang, G.; Liu, Y.; Ren, Y.; Zhao, Y.; Yu, Q.; Wang, Y.; et al. Toxicity of Nickel and Cobalt in Japanese Flounder. *Environ. Pollut.* **2020**, *263*, 114516. [CrossRef] [PubMed]
28. Di Lorenzo, F.; Burgos-Cara, A.; Ruiz-Agudo, E.; Putnis, C.V.; Prieto, M. Effect of Ferrous Iron on the Nucleation and Growth of $CaCO_3$ in Slightly Basic Aqueous Solutions. *CrystEngComm* **2017**, *19*, 447–460. [CrossRef]
29. Katsikopoulos, D.; Fernández-González, Á.; Carmelo, A.; Prieto, M. Co-Crystallization of Co (II) with Calcite: Implications for the Mobility of Cobalt in Aqueous Environments. *Chem. Geol.* **2008**, *254*, 87–100. [CrossRef]
30. González-López, J.; Fernández-González, Á.; Jiménez, A. Precipitation Behaviour in the System Ca^{2+}-Co^{2+}-CO_3^{2-}-H_2O at Ambient Conditions—Amorphous Phases and $CaCO_3$ Polymorphs. *Chem. Geol.* **2018**, *482*, 91–100. [CrossRef]
31. Zhang, X.; Guo, J.; Wu, S.; Chen, F.; Yang, Y. Divalent Heavy Metals and Uranyl Cations Incorporated in Calcite Change Its Dissolution Process. *Sci. Rep.* **2020**, *10*, 16864. [CrossRef]
32. Liu, Y.; Zou, Y. Experimental Study on the Relationship between Metal Ions and Formation of $CaCO_3$ Crystalline Fouling under Boiling Scaling System. *Heat Mass Transf. Stoffuebertragung* **2019**, *55*, 3077–3085. [CrossRef]
33. Lin, P.Y.; Wu, H.M.; Hsieh, S.L.; Li, J.S.; Dong, C.; Chen, C.W.; Hsieh, S. Preparation of Vaterite Calcium Carbonate Granules from Discarded Oyster Shells as an Adsorbent for Heavy Metal Ions Removal. *Chemosphere* **2020**, *254*, 126903. [CrossRef]
34. Rosenberg, P.E. Subsolidus Relations in the System $CaCO_3$-$FeCO_3$. *J. Sci.* **1963**, *261*, 683–689. [CrossRef]
35. Goldsmith, J.R.; Graf, D.L.; Witters, J.; Northrop, D.A. Studies in the System $CaCO_3$-$MgCO_3$-$FeCO_3$: 1. Phase Relations; 2. A Method for Major-Element Spectrochemical Analysis; 3. Compositions of Some Ferroan Dolomites. *J. Geol.* **1962**, *70*, 659–688. [CrossRef]
36. Neerup, R.; Løge, I.A.; Fosbøl, P.L. $FeCO_3$ Synthesis Pathways: The Influence of Temperature, Duration, and Pressure. *ACS Omega* **2023**, *8*, 3404–3414. [CrossRef] [PubMed]
37. Mejri, W.; Ben Salah, I.; Tlili, M.M. Speciation of Fe(II) and Fe(III) Effect on $CaCO_3$ Crystallization. *Cryst. Res. Technol.* **2015**, *50*, 236–243. [CrossRef]
38. Zeppenfeld, K. Prevention of $CaCO_3$ Scale Formation by Trace Amounts of Copper (II) in Comparison to Zinc (II). *Desalination* **2010**, *252*, 60–65. [CrossRef]
39. Iglikowska, A.; Bełdowski, J.; Chełchowski, M.; Chierici, M.; Kędra, M.; Przytarska, J.; Sowa, A.; Kukliński, P. Chemical Composition of Two Mineralogically Contrasting Arctic Bivalves' Shells and Their Relationships to Environmental Variables. *Mar. Pollut. Bull.* **2017**, *114*, 903–916. [CrossRef] [PubMed]
40. Rodriguez-Blanco, J.D.; Shaw, S.; Bots, P.; Roncal-Herrero, T.; Benning, L.G. The Role of Mg in the Crystallization of Monohydrocalcite. *Geochim. Cosmochim. Acta* **2014**, *127*, 204–220. [CrossRef]
41. Shannon, R.D. Revised Effective Ionic Radii and Systematic Studies of Interatomic Distances in Halides and Chalcogenides. *Acta Crystallogr. Sect. A* **1976**, *32*, 751–767. [CrossRef]

42. Graf, D.L. Crystallographic Tables for the Rhombohedral Carbonates. *Am. Mineral.* **1961**, *46*, 1283–1316.
43. De Villiers, J.P.R. Crystal Structures of Aragonite, Strontianite, and Witherite. *Am. Mineral.* **1971**, *56*, 758–767.
44. Swainson, I.P. The Structure of Monohydrocalcite and the Phase Composition of the Beachrock Deposits of Lake Butler and Lake Fellmongery, South Australia. *Am. Mineral.* **2008**, *93*, 1014–1018. [CrossRef]
45. Mikuš, T.; Patúš, M.; Luptáková, J.; Bancík, T.; Biroň, A. Mineralogical Characteristics of the Secondary Calcium Carbonates Association from the Špania Dolina-The First Occurrence of Monohydrocalcite in Ore Deposits in Slovakia. *Bull. Miner. Petrol.* **2017**, *25*, 318–326.
46. Hazen, R.M.; Hystad, G.; Golden, J.J.; Hummer, D.R.; Liu, C.; Downs, R.T.; Morrison, S.M.; Ralph, J.; Grew, E.S. Cobalt Mineral Ecology. *Am. Mineral.* **2017**, *102*, 108–116. [CrossRef]
47. Zhang, Q.; Yu, W.; Zhang, D.; Liu, M.; Wang, J.; Meng, K.; Yang, C.; Jin, X.; Zhang, G. Recent Advances on Synthesis of $CoCO_3$ with Controlled Morphologies. *Chem. Rec.* **2022**, *22*, e202200021. [CrossRef] [PubMed]
48. Pertlik, F. Structures of Hydrothermally Synthesized Cobalt (II) Carbonate and Nickel (II) Carbonate. *Acta Crystallogr.* **1986**, *C42*, 4–5. [CrossRef]
49. Li, H.; Duan, X.; Ma, J.; Zheng, W. A Controllable Ionic Liquid-Assisted Hydrothermal Route to Prepare $CoCO_3$ Crystals and Their Conversion to Porous Co_3O_4. *Cryst. Res. Technol.* **2012**, *47*, 25–30. [CrossRef]
50. Bermanec, V.; Sijarić, G.; Kniewald, G.; Mandarino, J.A. Gaspéite and Associated Ni-Rich Minerals from Veins in Altered Ultrabasic Rocks from Dubоštica, Bosnia and Herzegovina. *Can. Mineral.* **2000**, *38*, 1371–1376. [CrossRef]
51. Seguin, M.K. The Stability of Gaspeite in Inert Atmospheres and in Air. *Can. Mineral.* **1973**, *12*, 26–32.
52. Gaines, A.M.; Goldsmith, J.K. Crystal Chcmistry and Stability Relations in the System $MgCO_3$—$NiCO_3$. *Z. Für Krist.-Cryst. Mater.* **1971**, *133*, 432–444. [CrossRef]
53. Seidel, H.; Ehrhardt, H.; Viswanathan, K.; Johannes, W. Darstellung, Struktur Und Eigenschaften von Kupfer(II)-Carbonat. *ZAAC* **1974**, *410*, 138–148. [CrossRef]
54. Holme, E.A.; Henkes, G.A.; Tosca, N.J.; Rasbury, E.T.; Young, J.M.; Schaub, D.R.; Nekvasil, H.; Hurowitz, J.A. Experimental Constraints on Siderite Clumped Isotope Thermometry. *Geochim. Cosmochim. Acta* **2023**, *343*, 323–340. [CrossRef]
55. Glynn, P. Solid-Solution Solubilities and Thermodynamics: Sulfates, Carbonates and Halides. *Rev. Mineral. Geochem.* **2000**, *40*, 481–511. [CrossRef]
56. Gonzalez-Lopez, J.; Ruiz-Hernandez, S.E.; Fernandez-Gonzalez, A.; Jimenez, A.; Leeuw, N.H.D.; Grau-Crespo, R. Cobalt Incorporation in Calcite: Thermochemistry of $(Ca,Co)CO_3$ Solid Solutions from Density Functional Theory Simulations. *Geochim. Cosmochim. Acta* **2014**, *142*, 205–216. [CrossRef]
57. Maksimovic, Z.J. Resultats Preliminaires de l'examen Des Affleurements de Nickel Du Village de Ba, Pres de Ljig, Dans La Serbie Occidentale. *Recl. Trav. Acad. Derbe Sci.* **1952**, *23*, 21–48, 49–52.
58. Maksimovic, Z.J.; Stupar, J. La Calcite Nickelomagnesienne et l'aragonite de Rujevac (Village de Ba, Serbie Occidentale). *Recl. Trav. Acad. Derbe Sci.* **1953**, *33*, 220–221.
59. Ciurej, A.; Struska, M.; Wolska, A.; Szczerba, M.; Olszak, J. Copper-Bearing Mineralisation in the Upper Devonian Limestones: A Case Study from the Historical Teresa Adit in the Świętokrzyskie Mountains, Poland. *Minerals* **2023**, *13*, 54. [CrossRef]
60. Rosenberg, P.E. Subsolidus Relations in the System $CaCO_3$-$MgCO_3$-$FeCO_3$ between 350° and 550 °C. *Am. Mineral.* **1967**, *52*, 787–796.
61. Radha, A.V.; Navrotsky, A. Thermodynamics of Carbonates. *Rev. Mineral. Geochem.* **2013**, *77*, 73–121. [CrossRef]
62. Fosbøl, P.L.; Thomsen, K.; Stenby, E.H. Review and Recommended Thermodynamic Properties of $FeCO_3$. *Corros. Eng. Sci. Technol.* **2010**, *45*, 115–135. [CrossRef]